Article

Gypsum: From the Equilibrium to the Growth Shapes—Theory and Experiments

Dino Aquilano [1,*], Marco Bruno [1,2] and Stefano Ghignone [1]

1   Dipartimento di Scienze della Terra, Università degli Studi di Torino, Via Valperga Caluso 35, 10125 Torino, Italy; marco.bruno@unito.it (M.B.); s.ghignone@unito.it (S.G.)
2   NIS, Centre for Nanostructured Interfaces and Surfaces, Università degli Studi di Torino, Via G. Quarello 15/a, 10135 Torino, Italy
*   Correspondence: dino.aquilano@unito.it; Tel.: +39-338-4618780 or +39-338-9410297

Abstract: The gypsum crystals ($CaSO_4 \cdot 2H_2O$) crystallizes in a low symmetry system (monoclinic) and shows a marked layered structure along with a perfect cleavage parallel to the {010} faces. Owing to its widespread occurrence, as a single or twinned crystal, here the gypsum equilibrium (E.S.) and growth shapes (G.S.) have been re-visited. In making the distinction among E.S. and G.S., in the present work, the basic difference between epitaxy and homo-taxy is clearly evidenced. Gypsum has also been a fruitful occasion to recollect the general rules concerning either contact or penetration twins, for free growing and for twinned crystals nucleating onto pre-existing substrates. Both geometric and crystal growth aspects have been considered as well, by unifying theory and experiments of crystallography and crystal growth through the intervention of β_{adh}, the physical quantity representing the specific adhesion energy between gypsum and other phases. Hence, the adhesion energy allowed us to systematically use the Dupré's formula. In the final part of the paper, peculiar attention has been paid to sediments (or solution growth) where the crystal size is very small, in order to offer a new simple way to afford classical (CNT) and non-classical nucleation (NCNT) theories, both ruling two quantities commonly used in the industrial crystallization: the total induction times (t_{ind}^{total}) and crystal size distribution (CSD).

Keywords: equilibrium and growth shapes of gypsum; origins of gypsum-twins; epitaxy and homoepitaxy; crystal size distribution

1. Introduction

Writing an all-encompassing review paper on gypsum, $CaSO_4 \cdot 2H_2O$, represents a scientific task that transcends our capabilities. Despite having worked on this strategic crystal and its related mineral products for many decades, our gaze has always been directed with the attention of that type of researcher who takes equal account the "crystallography of the low-symmetry systems" and the complex phenomenon usually called "crystal growth". It will, therefore, not be a coincidence that in this review we will make constant reference to the School of Marseille, where Mrs. Simon [1,2], Kern [3–5], Boistelle [6–8], and many others have accustomed us to inextricably unite the "crystal bulk" to the "crystal surface" properties and to the "mother phase = environment" characteristics. This meant putting together the "classic 3D crystallography" with the "2D thermodynamics and kinetics" and the "fluid-dynamics" of the foreign phases, which can (or cannot) enter the crystal to become part of its own equilibrium E.S. and growth shapes G.S.

Essentially, for these reasons, we tried to deal with gypsum, aware that it would not make sense to treat gypsum without its twinning. Furthermore, from geologists, we understand every day that the lattice geometry is a consequence of the physics that they experience in epitaxy and in analogous phenomena (such as topo-and homo-taxy).

Hence, we conceived this review as composed by:

(i)   a short chapter giving the general rules for twinning, from the twin-geometry to the adhesion energy between the individuals composing a twin, to both its activation energy for nucleation and the related frequency;

(ii)   the basic distinction between the unicity of gypsum E.S. and its G.S. intrinsic plurality, as contained either in experiments (observation) or theory (calculation). A peculiar attention will be paid to the recent AFM observation on the cleavage {010} pinacoid, which changed our way of thinking on the gypsum growth mechanisms;

(iii)   the intervention of classic twinning (geometry) in the formation of straight twins, along the superposition of the homo-epitaxy (physics) when "curved" gypsum twins appear, as it usually occurs in geology;

(iv)   the origins of the gypsum twinning, for both "contact and penetration twins". The meaning of the Original Composition Plane (OCP) will be recovered, along with a twin analysis that takes into account all the literature data and an our recently published and complete study on the gypsum laws (for experiments and calculation);

(v)   a final paragraph outlining that gypsum usually present as an evaporite precipitating from brines and also is found as a scale in many industrial processes. Special care will be carried out for the growth of "very small sized crystals", leaving aside the beauty and ease of the large ones we encountered when working on their E.S. and G.S. Homo- and heterogeneous nucleation will be addressed along with the fundaments of classic (CNT) and non-classic (NCNT) nucleation theories. We will formulate, here and first as well, a practical application of foreseeing t_{ind}, i.e., the induction time needed to observe the microscopic and freshly precipitated crystals. Their crystal size distribution (CSD) will be analyzed, with a specific attention to the Dead Sea (Israel) phenomena: all the papers revolving around the PhD Thesis of A. Reiss [9] will be considered, having taken into account that all these studies [10–16] constitute the first example of how to scientifically tackle the problem of desertification.

2. General Rules for Twinning

2.1. Twinning (Geometry and Structure)

Let us recollect a classic definition of twinning (a crystal A on another crystal A in twinned position). Only one crystal species (A) is involved, and it can occur either during phase transitions or chemical reactions producing a crystal from other phases (vapour, solution, melt) and also from a pre-existent crystal phase. Hence, a twin can be viewed as an anomaly or a defect in respect to a homogeneous crystal. In any case, two twinned individuals are linked by a symmetry element (plane, axis), which cannot belong to the symmetry of the crystal A.

2.2. Specific Twin Energy

The specific twin energy can be obtained by applying Dupré's equation, starting from a general relation and recollecting that all the playing quantities are referred to the surface unity, and then should be expressed in erg $\times$ cm^{-2} [1,2].

Figure 1 explains the three stages needed to separate two distinct phases (A and B). The (AB) aggregate is made by two individuals (A and B), both having an area S. To separate them, a work $W_{sep}^{A/B}$ is needed. At this point, it is a matter of moving from the separation works to the specific surface energies. As an example to crystal A, its specific surface energy is defined: $\gamma_A = W_{sep}^A/(2S)$ according to the Born–Stern definition [17]. This general formula can be easily applied to a twin reaction: (A) is the parent crystal (P), while the other crystal (B) is the twinned (T) one. Accordingly, one realizes the transition from the separation works: $W_{sep}^{A/B} = W_{sep}^A + W_{sep}^B - 2E_{adh}^{A/B}$ to the specific surface energies, applied to the parent (P) and the twinned (T) crystals. The so obtained separation works are to be divided by their common area (2S), and hence one finally writes the Dupré's formula adapted to a twin: $\gamma_{PT} = \gamma_P + \gamma_T - \beta_{adh}^{P/T}$. For a deeper understanding of the general formula, readers are invited to observe both Figure 1 and Table 1.
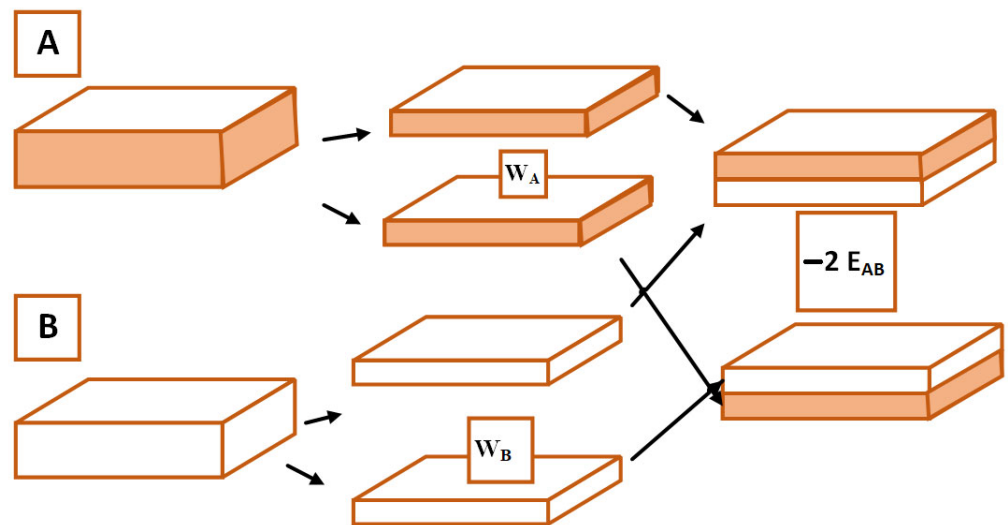
Figure 1. The separation work W_{AB} comes from the balance of two works: (i) that for separating each of the two phases (W_A, W_B) and (ii) the work recovered ($-2E_{AB}$) by coupling the two phases. To achieve the sense of "specific", all works must be divided by 2S. Table 1 is for twinning.

Table 1. The total expense ($W_{sep}^{P/T}$), as in the first row, equals the sum of two energies: that to separate crystal P (W_{sep}^{P}) and also crystal T (W_{sep}^{T}). Furthermore, we must consider the energy gain obtained by recomposing the twin $2E_{adh}^{P/T}/2S$, as from Figure 1. The second and third rows describe the transition from expenses and gain to the specific surface energy values.

Total Energy Expense	=	Energy (P) Expense	+	Energy (T) Expense	−	Total Energy Gain
$W_{sep}^{P/T}$	=	W_{sep}^{P}	+	W_{sep}^{T}	−	$2E_{adh}^{P/T}$
γ_{PT}	=	γ_P	+	γ_T	−	$\beta_{adh}^{P/T}$
γ_{twin}	=	γ_0	+	γ_0	−	$\beta_{adh}^{P/T}$

Thus, from Table 1, one achieves for a twin: $\gamma_P = \gamma_T = \gamma_0$. The specific energy of this aggregate depends on each constituent and on their adhesion energy, according to the Dupré's equation:

$$\gamma_{PT} = \gamma_{twin} = 2\gamma_0 - \beta_{adh}^{P/T} \tag{1}$$

The energy amount $2\gamma_0$ is the cohesion energy of the single crystal ($E_{cohes} = 2\gamma_0$), while γ_0 is nothing else than the specific surface energy of the original composition plane (OCP) of the twin. From the value of the specific adhesion energy, Equation (1) reads (Figure 2):
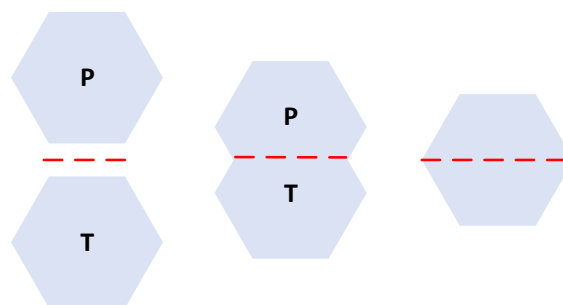

Figure 2. The drawing refers to Equation (1). Furthermore, it comments that the E.S. of a crystal embryo is able to make a twin. Case (a): $\gamma_{twin} = 2\gamma_0$, for two separated crystals. Case (c): $0 < \gamma_{twin} < 2\gamma_0$, for a non-perfect adhesion between P and T. Case (b): $\gamma_{twin} = 0$, when one cannot distinguish P from T.

(a) if $\beta_{adh}^{P/T} = 0$, any twin occurs, since $\gamma_{twin} = 2\gamma_0$ (two normal and separated crystals)

(b) if $\beta_{adh}^{P/T} = 2\gamma_0$, the adhesion is perfect, since $\gamma_{twin} = 0$ (a unique crystal obtains, since one cannot distinguish P from T)

(c) if $\beta_{adh}^{P/T} < 2\gamma_0$, adhesion will be non-perfect. Hence, $0 < \gamma_{twin} < 2\gamma_0$ (because twinning has its obvious cost)

Practically, the case (c) is the most interesting, also for gypsum. Since we are dealing with a "twin nucleation" we must examine the E.S. of its 3D-nucleus. Then, its 3D–activation energy (ΔG_{twin}^*), keeping in mind that we will consider, hereinafter, two ways: (i) a 3D-nucleation on a pre-existing crystal face; (ii) a 3D-nucleation on a free crystal face. We have just introduced, for that, the concept of the free energy variation (ΔG) as a function of the Born–Stern energies we used in Figure 1 and Table 1.

2.3. The Free 3D-Nucleation of an "Already Twinned" Crystal

We would like to draw the Gibbs–Wulff–Kaischew theorem [18–20] to represent a twin E.S. (contact twin, for the sake of simplicity). In Figure 3 the i-free faces are indicated by (γ_i^P, S_i, h_i), while the contact face is drawn as (γ_0, S_0, h_0). As usual, $\Delta\mu$ is the thermodynamic supersaturation, and V is the molecular volume of the crystal. Then, a system of (i + 1) equations is obtained:

$$\gamma_i^P - \frac{\Delta\mu}{2V}h_i = 0\frac{\gamma_i^P}{h_i} = \frac{\Delta\mu}{2V}(\gamma_i^P - \beta_{adh}) - \frac{\Delta\mu}{2V}h_0 = 0 \; \rightarrow \; \frac{\gamma_i^P - \beta_{adh}}{h_0} = \frac{\Delta\mu}{2V} \tag{2a}$$

that represents the Gibbs–Wulff–Kaischew theorem, as in Equation (2a), and the next Equation (2b):

$$\frac{\gamma_1^P}{h_1} = \frac{\gamma_2^P}{h_2} = \frac{\gamma_3^P}{h_3} = \cdots = \frac{\gamma_i^P - \beta_{adhes}}{h_0} = \frac{\Delta\mu}{2V} \tag{2b}$$
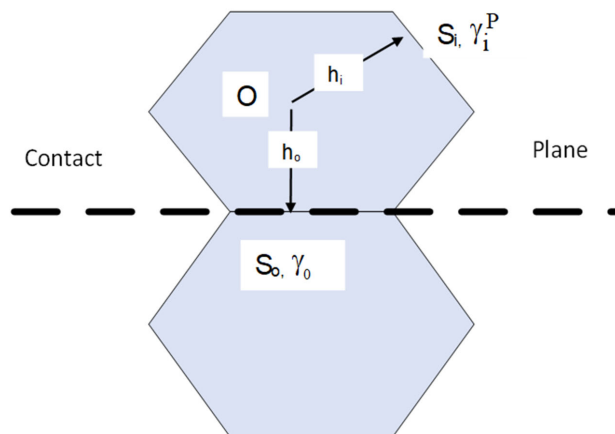

Figure 3. The Gibbs–Wulff–Kaischew theorem. In the Figure, the O point, called the Wulff's point [19], represents the completely random origin.

In both Equation (2a,b), the thermodynamic supersaturation is represented by $\Delta\mu = k_B$ T ln β, where k_B is the Boltzmann constant, T is in Kelvin degrees, and $\beta = (C/C_{eq}) = (1 + \sigma_v)$. Here, the exceeding supersaturation σ_v is the distance of the mother phase from its equilibrium. The actual solution concentration is C, while C_{eq} is its value at the equilibrium.

There is a way to evaluate the total surface energy (E_{tot}) and the total crystal volume (V_{tot}):

(i) $E_{tot} = 2 \times [\gamma_1 S_1 + \gamma_2 S_2 + \ldots] + \gamma_0 S_0$

(ii) The variation in V_{tot} is obtained through the Euler theorem (homogeneous functions of 3rd degree), which implies: $dV_{tot} = h_1 dS_1 + h_2 dS_2 + \ldots h_0 dS_0$. This geometric problem can be solved through the directing cosines ($\cos\mu_i$, $\cos\pi_i$, $\cos\tau_i$) of the segment normal to each i-face. The true independent variable became the (S_i) areas and,

hence, the distances (h_i) are abandoned. The minimum of E_{tot} obtains through the Lagrange's multipliers:

$$\lambda \times E_{tot} - dV_{tot} + \lambda_1 \times (dS_1 \times \cos\mu_1 + \ldots + dS_0 \times \cos\mu_0) + \lambda_2 \times (dS_1 \times \cos\pi_1 + \ldots + dS_0 \times \cos\pi_0) + \lambda_3 \times (dS_1 \times \cos\tau_1 + \ldots + dS_0 \times \cos\tau_0) = 0$$

The constants (λ, λ_1, λ_2, λ_3) can be easily calculated. In our reference frame, the equation of the i-face of the crystal reads: $x \times \cos\mu_i + y \times \cos\pi_i + z \times \cos\tau_i - h_i = 0$. Here, a point P (having λ_1, λ_2, λ_3 coordinates) can be always found. That is the Wulff-point, which assumes a distance (d_i) from the i-face of the crystal

$$d_i = h_i - \lambda_1 \times \cos\mu_i - \lambda_2 \times \cos\pi_i - \lambda_3 \times \cos\tau_i \tag{3a}$$

The distance (d_i) is now related to the constant (λ), implying $\rightarrow d_i = \lambda \times 2\gamma_i$, and Equation (3b) allows writing of the twin E.S., under the assumed condition: $0 < \beta_{adh} < 2\gamma_0$

$$\frac{\gamma_1}{d_1} = \frac{\gamma_2}{d_2} = \ldots = \frac{\gamma_0 - (\beta_{adh}/2)}{d_0} = \frac{1}{2\lambda} \tag{3b}$$

where the constant, λ, has been calculated from ΔG, according to the Gibbs–Thomson [18,21] method: $\lambda^{-1} = (2V/\Delta\mu)$. Once ($\Delta\mu$) and the molar crystal volume (V) are known, the crystal size is known as well.

So far, we evaluated our crystal through its specific adhesion energy $\beta_{adh}^{P/T}$ on the contact plane (OCP). Introducing the energy difference ($\Delta\phi$) between a simple crystal and a twinned one: $\Delta\phi = \gamma_0 - \left(\frac{\beta_{adh}}{2}\right)$, one obtains for different adhesion energies:

$$\beta_{adh}^{P/T} = 0 \rightarrow \Delta\phi = \gamma_0 ; \; 0 < \beta_{adh}^{P/T} < 2\gamma_0 \rightarrow 0 < \Delta\phi < \gamma_0 ; \; \beta_{adh}^{P/T} = 2\gamma_0 \rightarrow \Delta\phi = 0$$

2.4. Activation Free Energy for the Nucleation of a "Free" 3D-Twinned Embryo

A normal single crystal is made by N particles going from a dispersed to a condensed phase: their potential energy receives a negative ($-\Delta\mu$) transition. The volume term ($-N \times \Delta\mu$) opposes to the newly generated surface term $N^{2/3} \times \sum_i c_i\gamma_i$, having neglected both crystal edges and corners, and defined as (c_i) a shape factor for every i-face having a specific surface energy (γ_i). The variation in the Gibbs free energy (ΔG) reads:

$$\Delta G = -N \times \Delta\mu + N^{2/3} \times \sum_i c_i\gamma_i \tag{4a}$$

At the unstable equilibrium of this normal crystal: $d(\Delta G)/dN = 0$. Hence, a critical value (N = N*) is needed for which $N^* = \frac{8}{27} \frac{(\sum_i c_i\gamma_i)^3}{(\Delta\mu)^3}$. Thus: $\Delta G_{(N = N^*)} = \Delta G^*$ will assume, for a (spherical) normal crystal, the value:

$$\Delta G*_{normal} = \frac{(\sum_i c_i\gamma_i)^3}{(\Delta\mu)^2} \tag{4b}$$

A twin crystal is always made by N particles and the corresponding ΔG value will adapt himself. Hence ΔG will change to ΔG_{twin}, as from Equation (5a), Figure 4.

$$\Delta G_{twin} = -N\Delta\mu + N^{\frac{2}{3}}\left[2\sum_i c_i\gamma_i + 2\sum_j c_j\gamma_j + \gamma_0 c_0\right] \tag{5a}$$
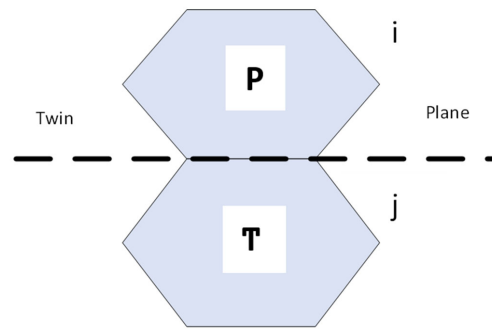
Figure 4. Twinned crystal: the free i-faces are not interested with the original contact plane (OCP-dashed line), and then can grow "homothetically". Instead, the j-faces adjacent to the OCP, will have an extension depending on the twin energy. The OCP has the constant (c_0) related to γ_0, its specific surface energy, as in Figure 3.

From the just cited Equation (5a), the N* size for which $d(\Delta G_{twin})/dN = 0$, should change as well:

$$\Delta G*_{twin} = \frac{4}{27} \frac{\left[2\sum_i c_i\gamma_i + 2\sum_j c_j\gamma_j + \gamma_0 c_0\right]^3}{(\Delta\mu)^2} \qquad (5b)$$

In case of twins ($0 < \beta_{adh}^{P/T} < 2\gamma_0$), it is always: $\Delta G*_{twin} > \Delta G*_{normal}$, as drawn in Figure 5a, where $\Delta\mu$ is maintained constant.
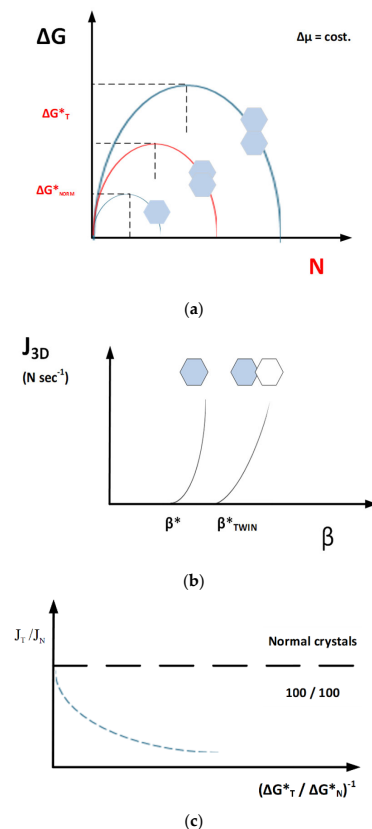
Figure 5. (**a**) The activation energy for twin nucleation $\Delta G*_{twin}$ is always higher than that needed to nucleate a normal crystal ($\Delta\phi = 0$) and lower than that due for two normal crystals; (**b**) The J_{3D} function: twins can be observed only at higher supersaturation values (β_{twin}^*) with respect to $\beta^* = \beta_{normal}^*$ needed to nucleate normal crystals; (**c**) The value (J_T/J_N) = 100% is reached only when: $\Delta G*_{twin} = \Delta G*$.

One should consider the 3D nucleation frequency (J3D) as well, which defines the number of nuclei generated per cm^3 and per second. It is correctly assumed that, for a normal crystal: $J^{3D}_{normal} \cong \exp(-\Delta G^*/k_B T)$, while $J^{3D}_{twin} \cong \exp(-\Delta G^*_{twin}/k_B T)$ for a twin.

3. Gypsum Crystal: From Equilibrium to Growth (or Dissolution) Forms

The crystal E.S. has been univocally defined by Wulff's theorem [19]:

$$\frac{\gamma_1}{h_1} = \frac{\gamma_2}{h_2} = \frac{\gamma_3}{h_3} = \ldots = \lambda^{-1} = \text{constant} \tag{6}$$

Here it presented in its simplest way, since it contains our needs:

- E.S. is always a closed and convex polyhedron.
- The constant λ does not depend on the *i*-face. Its value $\lambda^{-1} = (2V/\Delta\mu)$.
- The γ_i values were chosen as the minima among the i-faces.
- The h_i distances of each i-face from the Wulff's point of the polyhedron are always proportional to the related γ_i, as from Equation (6).
- From all the previous items, one must say that the E.S. cannot have a defined volume, due to Equation (6). It will be homothetic; its shape only depends on the calculated (or measured) γ_i values.

Then, one safety writes: E.S. $\rightarrow \gamma_i \rightarrow$ Wulff's polyhedron. The E.S. varies according to the adopted interatomic potential.

3.1. The Theoretical E.S. of Gypsum (CaSO$_4$ ·2H$_2$O)

- Simon and Bienfait [1] calculated the theoretical E.S. by searching the Periodic Bond Chains (PBCs) through the Hartman–Perdok (HP) method, [22] and considering the Coulomb interaction based on the electric (e) charge distribution: Ca = +2e, S = −0.3e, O (SO$_4^{2-}$) = −0.575e, H = +0.326e, O (H$_2$O) = −0.652e. Their E.S. is made by: 3 flats (F) forms: {010}, {120}, {011}.
- Heijnen and Hartman [23] modified the preceding Coulomb potential, by changing the charges on the two types of H$_2$O. Their E.S. is always made by the forms {010}, {120}, {011}, and {111}, even if {010} is less dominant with respect to the preceding case. In both the just quoted works [1,23], the surface was not relaxed (γ = γ unrelaxed). The surface relaxation was introduced only 20 years later.
- Massaro, Rubbo, and Aquilano [24] used two methods to calculate the surface profiles of gypsum: (i) searching for the PBCs through the HP method; (ii) a more advanced way, using the GDIS, 2005 programme [25]. In both cases, a general utility lattice programme [26] (GULP, 2003) was used to evaluate the γ values. This new synthesis allowed the attainment of richer and more isotropic E.S., for both unrelaxed and relaxed shapes. The final gypsum E.S. was made by four flat (F): {010}, {120}, {011}, {111} forms; two stepped (S): {100}, {122} forms, and one kinked (K): {102} form.

In a long period (1965–2010), the theoretic E.S. of gypsum increased in {hkl} forms, even if is not substantially changed. One may rightly ask which is the E.S. closest to the reality. The answer is simple: as for whatever kind of crystal, the gypsum E.S. has to be experimental and, hence, it will depend on T and P and on the medium where the observation has been made (vapour, solution, melt). See [3] for solution growth, as an example. Then:

$$\gamma_{theoretical} \neq \gamma_{experimental} \tag{7}$$

Moreover, we need to think that the {hkl} forms are considered as made by perfect surfaces; actually, dislocations could change their reality. Nevertheless, Equation (6) does not change, and one may write that both the stable E.S. and the unstable E.S. (as for nucleation) will depend only on the ratios among the γ_i values. Ultimately, only the Wulff's polyhedron dictates the E.S. unicity.

3.2. The Growth Shape (G.S.) of Gypsum

When a real crystal is immersed in a growing (dissolving) medium, the situation changes. It is out of the equilibrium and each of its (hkl) faces can grow (at supersaturation) or dissolve (unsaturation). Hence, a lot of new crystal–medium interfaces will appear, each presenting its own perfection level. Frank's discovery [27] imagined that a given (hkl) face could be disturbed by defects (edge and/or screw dislocations). Since then, the "ideal crystal" can be only an approximation of the "real crystal". To understand this, please look at a natural crystal face, having an averaged area = 1 cm^2, where up to 10^{14} dislocations can cross a face! This clearly proves that for a given crystal, the E.S. has nothing to do with its growth shape (G.S.).

The crystal face could be either perfect or imperfect. Moreover, its non-unicity will be further determined by its surrounding bulk-medium and thus by: (i) super(under) saturation ($\pm\Delta\mu$); (ii) temperature T and pressure p; (iii) diffusion within the boundary layer (bulk and/or surface); (iv) fluid-dynamics, outside the boundary layer

The cornerstones of the Burton–Cabrera–Frank (BCF) theory [27], despite the many additions, are not changed in time.

(a)   A perfect face (hkl) is populated by elementary steps of thickness d_{hkl}. Every step is made by atomic or molecular kinks in which the mother phase can enter, and steps can advance. This mechanism is nothing else than the "2D-nucleation".

(b)   An imperfect (hkl) face will be crossed by one screw dislocation (at least), which generates on its surface a permanent winding up of the exposed step. This face can normally advance through spiral growth, under the $\Delta\mu$ of the mother phase.

(c)   The growth units (G.U.s) can enter the kink-steps through their diffusion on the face surface or in the bulk of the mother phase. Further, it may happen that 2D-nuclei can form in between adjacent successive steps, so giving rise to a mixed mechanism: spiral growth + 2D nucleation.

3.2.1. On the {h0l} Growth Forms of Gypsum in Its [010] Zone

Following [28], the gypsum Space Groups (S.G.s) can be A2/a or C2/c. When looking at the {100} form, which is perpendicular to the glide plane, the stacking …AB… is made by the d_{200} slices (Figure 6). If two different PBCs, at least, should run within each of these slices, a screw dislocation crossing the face with its Burgers vector equal to the d_{200} thickness would generate a growth spiral having the stacking …AAAA…, corresponding to a new polytype of the S.G. A2. However, this is not allowed for the {100} form. Only the [001] PBCs develop within the d200 thickness corresponding to the period imposed by the S.G. A2/a since no bond can be found between two successive [001] PBCs in each d_{200} slice. These slices cannot be self-consistent layers able to spread in 2D, and the face will grow as a stepped one [29]. All the forms crossing normal to the glide plane should have S character: hence, polytypism cannot be setup in the [010] zone. Then, it could not be surprising that both {100} and {001} forms very rarely appear in the growth morphology of natural crystals and never belong to the habit of crystals grown from pure aqueous solutions. Concerning the change in growth mechanism, it can occur if an impurity could be adsorbed (either temporarily, or permanently in biominerals) in between two consecutive chains on the {100} form, and the face character [30] would change from S to F.
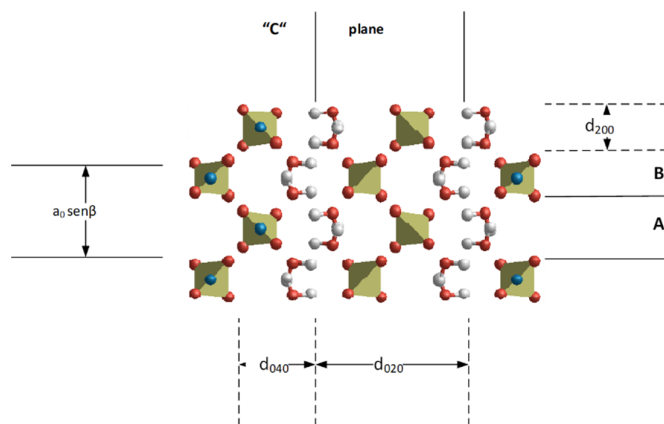
Figure 6. The homemade drawing, representing the gypsum projected along its [001] direction, is a strict application of the HP method [22]. Ca-atoms (blue) are located on the tetrahedra tops (and bottom), while SO_4^{2-} ions are square-shaped. Each SO_4^{2-} ion is only linked to its two water molecules. The limits of the d_{020} spacing are located in between the water molecules. The screw 2_1 axes, parallel to [010], lie in between A and B layers of thickness d_{200}. The d_{040} thickness is also indicated as a private communication by L. Pastero.

3.2.2. Going to the AFM Finer Observation of Gypsum in Its [010] Zone

We have just viewed the gypsum crystal in its complexity. Nevertheless, there is a finer way to approach its morphology, that is, by using more modern instruments to investigate the spirals growing on the {010} pinacoid, which is the most important form of gypsum (Figures 6 and 7).
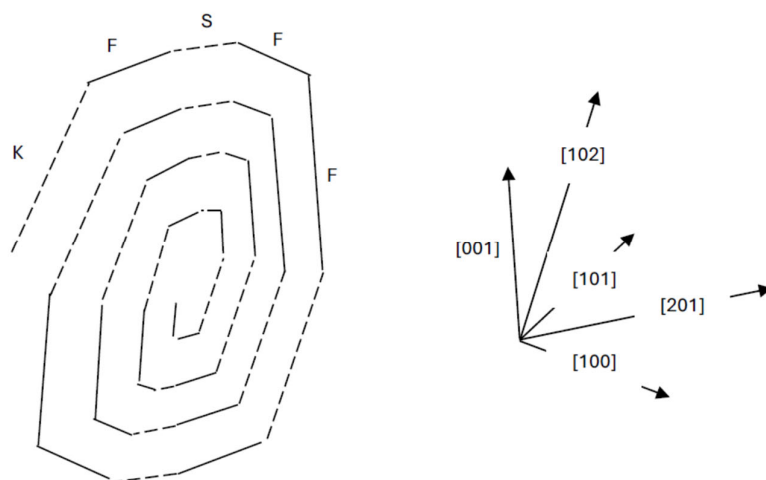

Figure 7. Scheme of an observed growth spiral along with the nanometric interstep distances and step directions. The measured step height is ~7.5 Å, which is the thickness $d_{020} = ½ b_0$. Working data: pure gypsum–water solutions; $T_{cryst.} = 80\ °C$; very low supersaturation: β = 1.062. Modified from [31].

The spiral arms in Figure 7 and those measured in the original work [31], indicate the true character of the forms lying in the [010] zone of gypsum:

(i)   straight steps are: [100], [001], [101] and then {001}, {100}, and {−101} are F forms
(ii)   kinked steps are: [201], [102] and then {−102} and {−201} are S or K forms.

Growth T plays an important role on the 2D-pattern shape. Actually, it is well-known that the entropic terms, contained in the expression of the edge energy, reduce its value and then increase the probability of a step to occur, both at equilibrium and in the growth patterns; accordingly, the polygonization of a growth pattern reduces with

increasing T, and hence the pattern becomes more rounded. These results represent a quantitative advancement in the knowledge of thermodynamic properties of gypsum and may have application in both geology and material science investigations. Moreover, this methodological approach could be a reference point for testing the validity of the simulation models of detailed surface studies in crystal growth from dilute aqueous solutions.

Summing up, the growth forms of Gypsum coming from rigorous observation of its faces are resultantly increased thanks to the optical macroscopy, microscopy, and AFM. The old (F) forms are: {010}, {120}, {011}, and {111}. The new F forms are: {001}, {100}, and {−101}, all belonging to the [010] zone (as in Figure 7); instead, {−102} and {−201} are stepped (S) or kinked (K) forms.

The theoretical and athermal E.S. of gypsum that was obtained by applying both the PBC and the GDIS methods is much more isotropic than those evaluated up to now. The E.S. is only determined by the ratios among the γ_i values of the forms and then is not a proof of the realism of the γ_i we calculated. The only available measurement that should be considered to check our reliability was obtained by Oglesby et al., 1976, who determined the {010} cleavage energy of gypsum as a function of the room air pressure [32]. They measured the cleavage energies as $\gamma_{010}^{-35\,°C}$ = 384 and $\gamma_{010}^{+65\,°C}$ = 360 erg cm^{-2}, while the averaged cleavage energy was $\gamma_{010}^{+25\,°C}$ = 355 ± 3 erg cm^{-2}. A linear fit gives: $\gamma = -0.26T + 440$ (erg cm^{-2}), where T is measured in Kelvin.

Previously, it has been shown that the thermal energy and entropy contributions to the surface free energy of a slab subjected to periodic 2D-boundary conditions, are not linear functions of T, but the combination (E$_{th}$-TS$_{th}$) is a nearly linear decreasing function of T, except at very low T. For that, the specific surface entropy can be estimated as 0.26 erg cm^{-2} K^{-1} at room T. Therefore, from the fit of the cleavage work, one obtains lower and upper bounds to the athermal γ at 0 K. The upper bound is just 440 erg cm^{-2}, i.e., the extrapolation of the experimental γ at 0 K; it includes the zero-point vibration energy of the surface; the lower one is γ calculated at 238.15 K, amounting to 378 erg cm^{-2} and includes both configuration and vibration contributions. The comparison with $\gamma_{010}^{0\,K}$ = 432 erg cm^{-2} here calculated, allows us to be quite confident in the force field we used [25,26].

It is also reasonable considering that the {010} form has the highest entropy, for the cleavage plane terminates with water molecules; the surface entropy being equal to about 0.26 erg cm^{-2} K^{-1} at room T, determines a γ decrease by about −77.48 erg cm^{-2}. Taking into account the values of the specific surface entropy of the ionic compounds, we can assume an approximate decrease by −30 erg cm^{-2} of the γ value for the most "anhydrous" gypsum surfaces such as, for instance, the {010} at room T. Thus, the shapes calculated at 0K do not change significantly at room T.

The method here that follows is a synthesis of two different points of view. The classic one, derived by the HP method, was aimed at predicting the crystal growth morphology: under this respect, the attachment energy (E$_{att}$) ratios measure the relative rate of crystallization of a d$_{hkl}$ layer over the various faces; although the method does not pretend to obtain the crystal E.S., it revealed fruitful to its determination. In the more modern way, the quest of potential surface configurations implemented in GDIS allows for a systematic scan of surface structures. When these structures can relax, as can be conducted with a code for energy minimization such as GULP, one can obtain more realistic crystal morphologies exhibiting a richer variety of forms

4. Origin of the Gypsum Twin Laws

In the following we aim to introduce the most important difference arising regarding the twin debate. The gypsum case is particularly sensible, owing to this crystal diffusion and reputation, but also to the imprinting turning point [4] due to Kern and Rehn who changed the way of thinking on twinning, moving from a geometric vision to the point of view of the crystal growth. Starting from previous considerations [5], the change reads:

Geometric definition: we have two twins, the first showing (100) as the twin plane, while the second one has the twin plane ($\bar{1}$01).

Growth definition: the twin genesis deeply varies. The contact (100) and ($\bar{1}$01) twins have these planes as the original composition planes (OCPs). The penetration (100) and ($\bar{1}$01) twins have the (010) plane as OCP, while the [001] and [101] directions became the original composition steps (OCS) on the just found (010) OCP.

The reconstructed drawing of Figure 8 has been obtained either by evaporating a Ca-sulphate solution, or by mixing two solutions containing $CaCl_2$ and H_2SO_4, respectively. Accordingly, the most frequent twin law is always the so-called Montmartre twin ($\bar{1}$01), which represents the opposite of the natural data, where the most frequent law is the "swallow tail" (100) twin law.
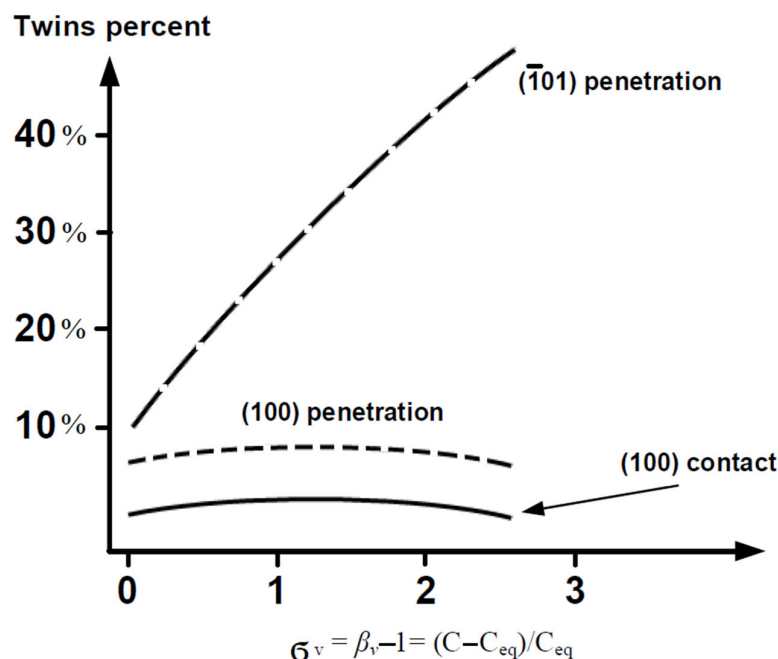

Figure 8. Historical gypsum twins, inspired by [4]. The twin percent (ordinate axis) is a function of both the twin laws and σ_v, the exceeding supersaturation. On the abscissa axis, one has: $\sigma_v = \beta - 1 = (C - C_{eq})/C_{eq}$, where C_{eq} is here related to T = 20 °C.

4.1. The Gypsum Mega-Crystals Born in Caves (Naica, Mexico and Pulpi, Spain)

In the Naica cave, faceted and transparent gypsum crystals grew, measuring an impressive 11 m (length) and 1 m (width). They were formed by a self-feeding mechanism, thermally driven by an anhydrite–gypsum transition (solution-mediated), at T = 54.5 ± 2 °C, over time [33–36]. Intriguingly, a similar formation mechanism was proposed for large and transparent gypsum crystal, selenite, (up to 2 m in length) found in the geode of Pulpí. However, data from fluid inclusions [37] indicate that Pulpí–gypsum precipitated at T = 20 ± 5 °C. The solubility in water, between gypsum and anhydrite, is higher at lower T (only if T < 54.5 °C). Consequently, gypsum crystals in Pulpí grew at a lower T when compared to those in Naica, resulting in a higher β_{bulk} value. This higher β_{bulk} value promotes massive nucleation, leading to many smaller crystals in the Pulpí cave [38]. This occurs when comparing the gypsum crystals in Pulpí with those in the Naica cave.

The growth of gypsum crystals via the anhydrite–gypsum transition is not completely organized, as concerns natural samples [33,36,37,39]. According to [38], gypsum has been synthesized using the experimental setup exploited to grow the silicate carbonate biomorphs [35]. Then, synthesis has been obtained via the anhydrite–gypsum self-feeding mechanism, at room T $\cong$ 20 ± 5 °C. Being closed and sealed to the atmosphere, the setup favours the reproduction of a closed, geode-like system. Hence, the laboratory allowed both to replicate the conditions under which gypsum precipitated in Naica and Pulpí caves, and to obtain the in situ monitoring of crystals by optical microscopy.

4.2. How Can We Distinguish in Lab the Origin of the Gypsum-Twin Laws?

The (100) contact twin law is the only well-recognized gypsum law, in natural environments, whereas it has never been observed through lab experiments. In the lab, the (100) and $(\bar{1}01)$ penetration twin laws are the most widespread [1,2,40]. Moreover, it is commonly accepted that: (i) α-amylase (an enzyme excreted into soils and water) triggers the precipitation of a gypsum twin habit (Montmartre twin) similar to those present in the Eocene deposits of the Paris Basin; (ii) the presence of CO_3^{2-} ions in the mother solution can promote the $(\bar{1}01)$ contact twin law of gypsum [41].

The question asked at the beginning of the paragraph was also posed in our lab; it has been recently well-answered by Cotellucci et al. who showed which ones of the gypsum twin laws can occur in pure solutions [40] at different evaporation rates (ER). They indicated that the (100) penetration twin law mainly occurs at slow evaporation rates (ER $\leq$ 0.030 g_{H2O}/h), i.e., low β values, whereas the opposite is true for the $(\bar{1}01)$ penetration law (ER > 0.030 g_{H2O}/h). Experiments further reveal another attribution for gypsum habits and twins. Prismatic single crystals and twins, following both the (100) contact and penetration laws, occur when only Ca^{2+} and SO_4^{2-} ions are dissolved in solution, at very low β values:1.3 (at 25 °C) $\leq$ β $\leq$ 1.4 (at 15 °C). According to this thinking, whether the anhydrite–gypsum dissolution process will be lab-reproduced at T > 25 °C (that means: β < 1.303), only blocky, prismatic single crystals and (100) contact twin law should be observed. A very low and constant over time β value is the key parameter to obtain these habits. Noteworthy, these conditions hold for the growth of the giant gypsum crystals in Naica [38], which exhibits only prismatic single crystals and gypsum twins following the (100) contact twin law.

Coming back to the few words written at the beginning, it took 60 years to pass from geometry to a thermodynamic–kinetic point of view, when working with the twinning. Once again, our short chapter proves that: evaporation rate (ER) → variable β regimes → variable $(C - C_{eq})$ values are the parameters determining the observed geometry, and not the vice versa. In other words, the pure geometry is a consequence, while the true cause stays in the complex thermodynamic–kinetics couple.

Finally, there is an elegant method recently found with the aim of distinguishing, through a simple optical microscope, the (100) from $(\bar{1}01)$ contact twins. Fluid inclusions captured during crystal growth assume a direction parallel to the [001] of the trapping crystal, since gypsum always grow [001] elongated, as in [40–43].

5. Curved Gypsum Crystals

The problems concerning the gypsum curvature are now 35 years old, having gone through the concepts of twinning, epitaxy, and homo-epitaxy. The first to bring some clarity to the question was the solution group of research [6,7,44,45] guided by R. Boistelle (CRMC2-Marseille). Here, they studied crystals in the lab, looking at the curvature with a crystallographic eye. The first precipitated crystals, formed at a high initial β value, were [001] elongated and showed neither defects nor curvature. Crystals of the second generation, grown at lower β, were generally curved with the only exception of those grown in the presence of Na^+ ions, as we will see later on. It was also certified that curvature can be syngenetic with crystal growth: at high β the ad/absorption kinetics of foreign molecules is too slow with respect to those of the main growth units building the crystal, whereas, at lower β, the crystal forms are progressively poisoned by the foreign impurities.

Some chemical influences can be considered to explain the crystal deformation:

- Na^+ ions do not induce any curvature, since they are small (1.24 Å) and do not form soluble complexes. If adsorbed, the crystal lattice is not disturbed
- Cd^{2+} and Mg^{2+} ions give rise to large soluble complexes and once incorporated, especially on the {120} form, they introduce important lattice defects. The amount of incorporated Cd^{2+} increases with increasing β; furthermore, it is worth saying that the initial β values needed for the gypsum nucleation increase with Cd^{2+} concentration.

The same occurs on the terminal {−111} faces, and this can explain the S-shaped form of curved crystals [6,7,44].

A few years later [45], from X-ray topography of gypsum, no screw dislocations were observed perpendicular to the {010} form. It took us almost twenty years to be able to make public that screw dislocations lines cross the {010} pinacoid [46]. Few growth hillocks were observed on the quoted faces, meaning that spirals do not make a significant contribution to the overall growth rate of the {010} form: hence, the 2D-nucleation can be considered as the main step generation mechanism.

Finally, only four years ago, patterns on the {010} form of gypsum crystals were studied in our lab, by AFM, under controlled T and low β values. From the hillocks formed by growth spirals generated by screw dislocations, the 2D-E.S. on the {010} form of gypsum was calculated [31].

The last papers published on the gypsum curvature come from our lab as well [40,41] and they are more complete with respect to past works. The ancient way of thinking the curved gypsum crystals as more or less rigid bodies showing one or two rotation angles [6,7] is now consigned to history (Table 2). The curved crystal habit can be seen as a continuous variation in the rotation angle between two successive compenetrated single individuals.

Table 2. Calculated rotation angles between two equivalent 010 gypsum lattices, along their corresponding area and angular misfits. The linear misfit is null, and the angular one is very small, for the rotation angle (a); this agrees with the observed occurrence frequency, which is much higher than that of mechanical twin, corresponding to the rotation angle (b).

Rotation Angle	Lattice 1	Lattice 2	Linear Misfit (Δ%)	Angular Misfit (°)
(a) 18°58′	[401] 5[001]	[402] [−204]	0 0	2°3′
(b) 23°53′	[302] 4[001]	[301] [−203]	6.4 1.9	1°38′

A new criterion to understand the curved habit of gypsum has been recently found [40]: the evaporation rate (E.R.) effect on gypsum habit. This effect was investigated by carrying out four batches of experiments at four different E.R., and different gypsum habits as a function of E.R. have been detected. By increasing the E.R., the (101) penetration twins are favoured with respect to the (100) penetration ones, and the (101) twin law can occur with two different habits whose occurrence frequencies are related to the E.R. as well. Previous experiments disclosed the formation of the well-known (100) and (101) twinned gypsum crystals in the presence of organic molecules characteristic of sedimentary environments. Consequently, these twin laws can be detected in evaporitic sedimentary environments. Aimed at favouring researchers to identify the twin laws of gypsum, the measurement of the crystal aspect ratio (length/width crystal ratio) has been proposed [40,41] as a potentially fast and useful tool to distinguish between (100) and (101) penetration twins. At higher evaporation rates (ER ≥ 0.79 g/h), curved crystals exhibit both "symmetric" and "asymmetric" curvatures. Based on crystallographic considerations, Rinaudo et al. [6,7] suggested that a twinning mechanism may promote the symmetric curvature, whereas Cotellucci et al. hypothesized [40] an homoepitaxy for the asymmetric one. Moreover, until today, the crystal curvature has been related to impurities absorption, but another growth attribution has been here documented, independent from the chemical environment and only related to β values. These experimental findings provide the first evidence of different gypsum habits as a function of E.R. in a pure system. Acicular single crystals, curved crystals, (100), and (101) penetration twins are the habits detected. When the effect of additives on gypsum is explored by performing growth experiments, and when

different habits are analyzed in evaporitic environments, this wide array of habits should be considered.

Summing up, we would like to add personal considerations. The number of "twin laws" of gypsum is necessarily limited and confined to well-known literature already described within the present review paper. Nonetheless, a new way of thinking [40] has been introduced: the observed phenomena giving origin to the "continuous rotation angles" occur in the 010—gypsum plane and, consequently, can be attributed only to homo-epitaxy (gypsum 010-plane growing on gypsum 010-plane means: crystal A/crystal A growth). After the recent papers published by our research group on the homo-epitaxy of aragonite and calcite, there is a good reason to be proud of having added gypsum to the enriching family of "homo-epitaxial crystals".

6. Gypsum Brines

The recurrent Ca-sulphates (gypsum, bassanite, and anhydrite) differ by their hydration degree. Gypsum is the most common sulphate mineral on Earth, spanning from Africa and Asia, to America, Australia, and even Antarctlia. It is an evaporitic mineral that predominantly precipitates from brines in a wide geographical ranged scale and is found as well in many processes that utilize or produce industrial brines. In these processes, such as desalination and the production of oil and hydrothermal energy, gypsum precipitation under saline conditions also occurs and forms a scale that may clog membranes, pipes, and boreholes, affect aquifers and reservoirs, and can result in the temporary halting of production. Thus, insights into gypsum formation can be used to better understand its natural occurrence and improve industrial practises. It is also plain to see that over the last decade, thermodynamics, nucleation along with crystal growth mechanisms and kinetics have been widely studied, to better understand how these factors shape the gypsum morphology. Its precipitation under saline and hypersaline conditions has been the focus of several studies, but thermodynamic data are derived mostly from experiments with artificial solutions that have limited background electrolytes with Ca^{2+}/SO_4^{2-} ratios being quite similar to the 1:1 ratio in gypsum. Furthermore, the majority of kinetic processes are still derived from lab experiments made at low ionic strength. Thus, both natural gypsum and industrial processes are still less well-known. To prevent the gypsum scale formation (as other minerals), scale inhibitors are often added in industry to brines; their addition increases operational costs and introduces undesired consequences in nature. Furthermore, modern advanced techniques (like AFM, TEM, plus small and wide-angle X-ray scattering, such as SAXS/WAXS) are increasingly used to study the early precipitation and growth stages. Nonetheless, the chemical complexity of brines becomes a challenge when applying both these old and new techniques.

Our work here focuses on the precipitation of gypsum brines. First, ionic strength, brine composition, and T effects on thermodynamics are broadly discussed, since all these brine properties have been shown by recent micro-macroscopic observations that tried to explain both the morphology and crystal size distribution. Secondly, we tried to highlight the micro-macroscopic discrepancies by studying low and high ionic strengths. The special challenges posed by experiments with brines are also discussed. Then, starting from contemporary literature, we will outline further research needed to improve our understanding of both natural gypsum precipitation and its industrial settings.

As there is a wealth of ideas in this research area, which has generated certain confusion, we will try to remedy this following a principle of order.

6.1. Thermodynamics

Determination of Saturation, Solubility, and Activity.

Here, we state that one needs to get rid of some terms already used [12,16] in thermodynamics:

$$\mathrm{DS}_{\mathrm{gypsum}} = \frac{\mathrm{IAP}}{\mathrm{K}_{\mathrm{eq}}} \tag{8}$$

where (i) DS_{gypsum} indicate the saturation degree of a gypsum solution, (ii) is the thermodynamic solubility, $K_{eq} = IAP_{eq}$, which is the product of the ionic activities and represents the value of IAP, at the equilibrium. Once again, we prefer using the definition through the free energy variation (ΔG) in the system:

$$\frac{\Delta G}{RT} = \ln\left(\frac{IAP}{K_{eq}}\right) \quad (9)$$

According to Equations (8) and (9) one can immediately writing that:

$\left(\frac{IAP}{K_{eq}}\right) = 1 \rightarrow \Delta G = 0$, means the system crystal/solution in equilibrium $\rightarrow DS_{gypsum} = 1$

$\left(\frac{IAP}{K_{eq}}\right) < 1 \rightarrow \Delta G < 0$, if crystals dissolve in the unsaturated solution $\rightarrow DS_{gypsum} < 1$

$\left(\frac{IAP}{K_{eq}}\right) > 1 \rightarrow \Delta G > 0$, when crystal grows in supersaturated solution $\rightarrow DS_{gypsum} > 1$

The solubility (C_s) of a mineral is the molal concentration of that mineral dissolved in a solution at equilibrium. As an example, in the case of gypsum at equilibrium, the case ($DS_{gypsum} = 1$) has to be applied. Hereinafter, one should be cautious when using the term Ω because, in the following, we will use Ω (m^3 × mol^{-1}) to represent the volume of the G.U. inside every kind of crystal, and not the saturation degree (DS_{gypsum}) of a gypsum solution.

6.2. Gypsum Precipitation in Saline Environments: Mechanisms and Rates

6.2.1. Pathways of Nucleation

As outlined elsewhere in this review, during nucleation, the growth units (G.U.s) are dissolved in a supersaturated solution and react to form a crystal, according to two main schematic theories: a "classical-CNT" or a "non-classical-NCNT" pathway. According to CNT, a nucleus with a structure similar to the macroscopic bulky crystal is formed. A specific interfacial tension γ arises between such metastable nuclei and the solution. These n-sized nuclei may dissolve or further react with the monomers, so further increasing the (ΔG) value of the system. As a nucleus surpasses its critical size n*, being (n ≥ n*) and consequently $\Delta G < \Delta G^*$, the activation energy for nucleation ΔG^* is reached and the nucleus will become a stable crystal, as in our Figure 5. Following the CNT, nucleation is a single-step process in which a solid forms with the crystal bulk properties. When foreign nuclei are absent in the solution, one obtains homogeneous nucleation. If the new forming nuclei are generated on pre-existing nuclei or other surfaces, then γ is lowered, and hence ΔG^* as well: the nucleation is hetero-directed, and we will call it heterogeneous nucleation. As an example, dust nanoparticles in solution act as nuclei for gypsum, and nucleation is practically heterogeneous.

Concerning CNT, we are interested [47] to correctly show the homogeneous 3D-nucleation frequency (J_{3D} = nuclei × sec^{-1} and per solution unit volume).

$$J_{3D-homo} = A_k \exp\left\{-(16\pi/3)\,\frac{\Omega^2\gamma_{sl}^3}{k_BT(\Delta\mu)^2}\right\} \quad (10)$$

which stands for a spherical nucleus, so giving rise to the constant = $(16\pi/3)$. We improved Equation (10): the constant $A_k \approx 10^{25}$; Ω is the volume of the G.U. in the crystal and equals 7.469×10^{-5} (m^3 × mol^{-1}); γ_{sl} is the specific interface solution/crystal energy; k_B is Boltzmann's constant; T is the Kelvin temperature; and $\Delta\mu = (k_B T)$ is ln β, where $\beta = (a/a_{eq})_{T,P}$ is here expressed through the solution activities, measured at constant T and pressure.

As a crude approximation, we can accept that the frequency of heterogeneous nucleation differs from the homogeneous one owing to a new specific interfacial solution/crystal energy [9,16]. It was also invoked [48] that hetero-nuclei lower the interfacial solution/crystal energy, in such a way that $\gamma_{hetero}^3 = \gamma_{sl}^3 \times (0.1 - 0.3)$. The just found gypsum correction factor: $0.1 < f(\theta) < 0.3$ is for heterogeneous nucleation, necessarily being

$0 < f(\theta) < 1$. NCNT is any nucleation process that does not follow the just described path. Observations made at the nano- and micrometric scales demonstrate that nucleation often begins with "pre-nucleation" clusters reacting to form the stable bulk crystal. Hence, NCNT involves at least two steps.

The rate of nucleation, J_{3D}, is difficult to measure. Practically, experiments on nucleation kinetics measure the induction time (T_{ind}), which is the time passing between the initial β value and the ability to detect the new phase. This obviously depends on the method of detection and, thus, T_{ind} is method specific. However, it was assumed that the faster the nucleation rate, the shorter is T_{ind}. This means that the relationship [49] between J_{total}, the total nucleation frequency, and T_{ind} could be:

$$T_{ind} = \frac{K}{J_{total}} \tag{11}$$

where K is a coefficient of proportionality. Equation (11) can be used to determine the effect that solution properties have on the frequency of nucleation. Kinetic models based on this equation accurately predict the gypsum T_{ind} under saline and hypersaline conditions. Moreover, when coupled with crystal growth equations, CNT-based models were able to describe the change in the concentration of SO_4^{2-} ions over the course of gypsum precipitation, from the initial β value until chemical equilibrium was attained.

For practical purposes it can be useful the approach recently followed when evaluating the J_{total} due to both homo- and heterogeneous nucleation [9,16]. The original intuition comes from [49], where the coefficient A_k in Equation (10) is simply $A = b \times C_s$. Here, we like to repeat that C_s is the mineral solubility, i.e., its molal concentration in solution at equilibrium ($DS_{gypsum} = 1$). The coefficient (b) is nothing else, and the proportion between homo (b_{homo}) and heterogeneous (b_{het}) nucleation is to be adopted to evaluate the induction time that one measures, as the nucleation frequency reaches J_{total}. In this way, we modified the total induction time and wrote:

$$T_{ind}^{total} = \frac{K}{C_s} \times \frac{1}{b_{homo}\exp\left\{-(f_{homo})\frac{\Omega^2\gamma_{sl}^3}{k_BT(\Delta\mu)^2}\right\} + b_{het}\exp\left\{-(f_{het})\frac{\Omega^2\gamma_{het}^3}{k_BT(\Delta\mu)^2}\right\}} \tag{12}$$

In Equation (12), we only introduced new terms in order to complete its signification. They are: (i) the two constants (f_{homo}) and (f_{het}), characterizing the factor forms of the respective homo and hetero-nuclei; ii) the term $\gamma_{het}^3 = \gamma_{sl}^3 \times (0.1 - 0.3)$, as it was just anticipated when considering the hetero-nucleation in place of the homo-nucleation.

Gypsum commonly precipitates from evaporated seawater in lagoon beach sabkhas [50]. When the evaporation factor value >2.8, β can, thus, work even if, at low β, the kinetics of the reaction is very slow. As a matter of fact, the calculated induction time is longer than the age of the Earth when the evaporation seawater factor reaches the value of $\approx$3. The induction time becomes reasonable (few years) only if the evaporation factor approaches the value of $\approx$3.3, as it may be seen in [13]. An interesting and more realistic case can be found [13] in the mass balance on the Dead Sea. These Authors, starting from a preceding calculation [10] estimated that the annual evaporation factor of the Dead Sea brine in the northern basin varies between 1.003 and 1.005, whereas the evaporation factor of the Dead Sea brine in the evaporation ponds at the southern basin reaches near 1.6. This large difference between the measured evaporation factors is a result of the difference in the water bodies' volume to surface area ratio.

To date, there is no mathematical framework to calculate $J_{nucleation}$ based on NCNT models. However, while nucleation is a micro-phenomenon, Equation (12) is derived from bulk properties (i.e., γ, T, β, etc.). At the nanoscale, these thermodynamic and kinetic properties may differ from the bulky ones. Moreover, Equation (12) does not consider the number of steps during nucleation. Nevertheless, it is well known that one should have handle a robust mathematical framework for treating nucleation kinetics, whether the process arises either via the CNT or NCNT path.

6.2.2. Crystal Size Distribution (CSD) of Gypsum and Its Implications

The CSD of a given population summarizes the mutual effects of chemical (nucleation, growth, and dissolution) and mechanical (agglomeration or breakage of crystals) processes affecting the individual crystals. Thus, the CSD can interpret the geology, who oversaw the history of the crystal population. Since gypsum can form undesired scale as well, its CSD becomes important in various industrial processes. As an example, the gypsum CSD determines the filtration rate during wet industrial processes in which the mineral precipitates. Accordingly, understanding the mutual interaction between chemistry, physics, and the mechanisms that control gypsum shape and size, may help adopt new protocols to obtain the precipitation process towards the preferable CSDs.

In this regard, we aim at outlining that the GS shapes of gypsum single crystals have been discussed in other words, within this paper; in fact, the very small gypsum sizes studied in CSDs have nothing to do with the beautiful ones we described when dealing with well-formed single crystals, by applying the BCF models.

Looking to the not distant future of our lakes or ponds, the Dead Sea might be a very useful example, especially if we would consider that gypsum-CSD will determine if the crystals will quickly settle to the bottom or remain suspended and whiten the surface waters. This is a "Lognormal size distribution" in which the logarithm of the size is normally distributed, as it usually occurs in natural environments, on desalination membranes, and from batch solutions of hypersaline brines [51–54].

Today, all the growth models that relate the growth rate to the distance from equilibrium cannot explain the gypsum CSD, since only some decades ago it has been realized that geologic samples, including grain size in sediments and minerals in rocks, often follow or closely approximate a lognormal distribution. Middleton [52] had made the first rigorous attempt to explain the development of such CSD within a geological context and showed that a lognormal distribution can be mathematically modelled in several ways, describing it in sediments. However, Middleton noted that his model pre-supposed assumptions not necessarily valid from the underlying physical process.

Recently, it has been suggested that agglomeration of particles during the early stages of gypsum precipitation may be a mechanism affecting the final CSD. This suggestion is in agreement with the observation [55] that gypsum crystals are meso-crystals. However, the extent to which agglomeration shapes the final CSD, still requires further study [11,14,56].

7. Conclusions

Even if we wanted to privilege the educational aspects, some research foundations have been acquired: this is what we intend to discuss in these review conclusions. Sharp distinctions have been made between equilibrium and growth shapes of gypsum, along with a practical presentation of the related experimental and theoretical results. Hence, we took the opportunity to highlight how only modern experimentation (like the AFM measurements) has made it possible to improve knowledge of the growth mechanisms of important surfaces, as the {010}-pinacoid, and of the forms in zone with the [010] axis. The integrated study between crystallography and geology has allowed us to delve deeper and discriminate between different gypsum twins, for both contact and penetration, by using concepts such as the capture of fluid inclusions (F.I.) and their orientation in the gypsum crystal, together with the evaporation rate (E.R.) and the ionic strength (I.S.) of the mother solutions.

In this regard we are pleased to remember that, for the first time, it has been focused that: twinning, epitaxy, homo-epitaxy and topo-taxy can coexist in gypsum, thanks to our fruitful studies (since many years and also today) on the rich gypsum twin morphology.

Taking advantage of our experience to deepen the study of gypsum brines, we were allowed to improve mathematical tools needed to understand both nucleation and growth of very small gypsum crystals, in order to better quantify the knowledge of the induction times and of the CSD.

Finally, this overview was necessary to address some of the new issues, only partially resolved:

- gypsum and copolymers, including all the products needed in cultural heritage;
- all the non-published interfaces among gypsum and the most common Ca-carbonates (aragonite-calcite)
- the transition: gypsum → brushite $CaHPO_4 \cdot 2H_2O$ → ardealite $Ca_2 \cdot HPO_4 \cdot SO_4 \cdot 4H_2O$
- the transition: gypsum → brushite → (Hap)-hydroxyapatite $[Ca_5(PO_4) \cdot 3OH]$ along with other biomimetic minerals

A lot of minerals concerning the past-life and the organism living today may be the interest for future studies on "gypsum brothers". Many thanks to you, and remember: "...our work has just begun"!

References

1. Simon, B.; Bienfait, M. Structure et mécanisme de croissance du gypse. *Acta Crystallogr.* **1965**, *19*, 750–756. [CrossRef]
2. Simon, B. Contribution à L'étude de la Formation des Macles de Croissance. Ph.D. Thesis, Aix Marseille Université, Marseille, France, 1968.
3. Bienfait, M.; Kern, R. Etablissement de la forme d'équilibre d'un cristal par la méthode de Lemmlein-Klija. *Bull. Minéral.* **1964**, *87*, 604–613.
4. Kern, R.; Rehn, B. Étude expérimentale de la formation des macles de croissance du gypse. *C. R. L'acad. Sci. Paris* **1960**, *261*, 130.
5. Curien, H.; Kern, R. Macles par contact et par pénétration. Essai d'interprétation causale Bull. *Bull. Minéral.* **1957**, *80*, 111–132.
6. Rinaudo, C.; Franchini-Angela, M.; Boistelle, R. Gypsum crystallization from cadmium-poisoned solutions. *J. Cryst. Growth* **1988**, *89*, 257–266. [CrossRef]
7. Rinaudo, C.; Franchini-Angela, M.; Boistelle, R. Curvature of gypsum crystals induced by growth in the presence of impurities. *Mineral. Mag.* **1989**, *53*, 479–482. [CrossRef]
8. Boistelle, R.; Lopez-Valero, I. Growth units and nucleation: The case of calcium phosphates. *J. Cryst. Growth* **1990**, *102*, 609–617. [CrossRef]
9. Reiss, A.G. The Coupling Between Gypsum Nucleation and Crystal Growth: Implications for the Possible Whitening of the Dead Sea. Ph.D. Thesis, Ben-Gurion University of the Negev, Beersheba, Israel, 2020.
10. Lensky, N.G.; Dvorkin, Y.; Lyakhovsky, V.; Gertman, I.; Gavrieli, I. Mass and energy balance of a hypersaline lake: The Dead Sea. *Water Resour. Res.* **2005**, *41*, 1–13. [CrossRef]
11. Reznik, I.J.; Gavrieli, I.; Ganor, J. Kinetics of gypsum nucleation and crystal growth from Dead Sea brine. *Geochim. Cosmochim. Acta* **2009**, *73*, 6218–6230. [CrossRef]
12. Reznik, I.J.; Gavrieli, I.; Antler, G.; Ganor, J. Kinetics of gypsum crystal growth from high ionic strength solutions. A case study of Dead Sea–seawater mixtures. *Geochim. Cosmochim. Acta* **2011**, *75*, 2187–2199. [CrossRef]
13. Reznik, I.J.; Ganor, J.; Gruber, C.; Gavrieli, I. Towards the establishment of a general rate law for gypsum nucleation. *Geochim. Cosmochim. Acta* **2012**, *85*, 75–87. [CrossRef]
14. Reiss, A.G.; Gavrieli, I.; Ganor, J. The Morphology of Gypsum Precipitated Under Hyper-Saline Conditions. Preliminary Results from Dead Sea-Red Sea Mixtures. *Procedia Earth Planet. Sci.* **2017**, *17*, 376–379. [CrossRef]
15. Reiss, A.G.; Ganor, J.; Gavrieli, I. Size Distribution and Morphology of Gypsum Crystals Precipitating from Hypersaline Solutions. *Cryst. Growth Des.* **2019**, *19*, 6954–6962. [CrossRef]
16. Reiss, A.G.; Gavrieli, I.; Rosenberg, Y.O.; Reznik, I.J.; Luttge, A.; Emmanuel, S.; Ganor, J. Gypsum Precipitation under Saline Conditions: Thermodynamics, Kinetics, Morphology, and Size. *Minerals* **2021**, *11*, 141–177. [CrossRef]
17. Born, M.; Stern, O. Oberflächenenergie von Kristallen. *Ber. Berl. Akad.* **1919**, *48*, 901–920.
18. Gibbs, J.W. On the equilibrium of heterogeneous substances. In *The Scientific Papers of J.W. Gibbs, I.*; Longmans, Green &Co.: London, UK, 1906.
19. Wulff, G. Zur Frage der Geschwindigkeit des Wachstums und die Auflösung der Kristallfläken. *Zeit. Kristall.* **1901**, *34*, 449–530.
20. Kaischew, R. Gleichgewichtsform eines Kristalls auf einer Unterlages. *Bull. Acad. Sci. Bulg. Sér. Phys.* **1951**, *2*, 191–203.
21. Thomson, J.J. *Applications of Dynamics to Physics and Chemistry*; Macmillan and Co.: London, UK, 1888.
22. Hartman, P.; Perdok, W.G. On the relation between structure and morphology. I, II, III. *Acta Cryst.* **1955**, *8*, 49–52, 521–529. [CrossRef]

23. Heijnen, W.M.M.; Hartman, P. Structural morphology of gypsum (CaSO$_4$· 2H$_2$O), brushite (CaHPO$_4$· 2H$_2$O) and pharmacolite (CaHAsO$_4$· 2H$_2$O). *J. Cryst. Growth* **1991**, *108*, 290–300. [CrossRef]

24. Massaro, F.R.; Rubbo, M.; Aquilano, D. Theoretical Equilibrium Morphology of Gypsum (CaSO$_4$ · 2H$_2$O). 1. A Syncretic Strategy to Calculate the Morphology of Crystals. *Cryst. Growth Des.* **2010**, *10*, 2870–2878. [CrossRef]

25. Fleming, S.; Rohl, A.L. GDIS: A visualization program for molecular and periodic systems. *Zeit. Kristall.* **2005**, *220*, 580–584. [CrossRef]

26. Gale, J.D.; Rohl, A.L. The General Utility Program (GULP). *Mol. Simul.* **2003**, *29*, 291–341. [CrossRef]

27. Burton, W.K.; Cabrera, N.; Frank, F.C. The growth of crystals and the equilibrium structure of their surfaces. *Philos. Trans. R. Soc. A* **1951**, *243*, 299–358.

28. De Jong, W.F.; Bouman, J. Das reziproke und das Bravaissche Gitter von Gips. *Z. Krist.* **1939**, *100*, 275–276. [CrossRef]

29. Aquilano, D.; Pastero, L.; Veesler, S.; Astier, J.P. Space groups of crystal and polytypism. The interplay among symmetry elements, face characters and screw dislocations. In Proceedings of the (2003) Joint Italo-French Meeting "Crystal Growth: From Basic to Applied", Accad. Lincei, Roma, Italy, 2–3 October 2002; pp. 21–36.

30. Hartman, P.; Kern, R. Le changement de faciès par adsorption et la théorie des PBC. *C. R. Acad. Sci. Paris* **1964**, *258*, 4591–4593.

31. Criado-Reyes, J.; Pastero, L.; Bruno, M.; García-Ruiz, J.M.; Aquilano, D.; Otálora, F. Equilibrium Shape of 2D Nuclei Obtained from Spiral Hillocks on {010} Form of Gypsum. *Cryst. Growth Des.* **2020**, *20*, 1526–1530. [CrossRef]

32. Oglesby, M.L.; Gutshall, P.L.; Phillips, J.M. Cleavage surface energy of selenite. *Am. Mineral.* **1976**, *61*, 295–298.

33. García-Ruiz, J.M.; Villasuso, R.; Ayora, C.; Canals, A.; Otálora, F. Formation of natural gypsum mega-crystals in Naica, Mexico. *Geology* **2007**, *35*, 327–330. [CrossRef]

34. García-Ruiz, J.M.; Canals, A.; Ayora, C. Gypsum mega-crystals. In *McGraw-Hill Yearbook of Science and Technology*; McGraw-Hill Book Co.: New York, NY, USA, 2008.

35. García-Ruiz, J.M.; Melero-García, E.; Hyde, S.T. Morphogenesis of Self-Assembled Nanocrystalline Materials of Barium Carbonate and Silica. *Science* **2009**, *323*, 362–365. [CrossRef]

36. Krüger, Y.; García-Ruiz, J.M.; Canals, À.; Martí, D.; Frenz, M.; Van Driessche, A.E.S. Determining gypsum growth temperatures using monophase fluid inclusions—Application to the giant gypsum crystals of Naica, Mexico. *Geology* **2013**, *41*, 119–122. [CrossRef]

37. Canals, À.; van Driessche, A.E.S.; Palero, F.; García-Ruiz, J.M. The origin of large gypsum crystals in the Geode of Pulpí (Almería, Spain). *Geology* **2019**, *47*, 1161–1165. [CrossRef]

38. Otálora, F.; García-Ruiz, J.M. Nucleation and growth of the Naica giant gypsum crystals. *Chem. Soc. Rev.* **2014**, *43*, 2013–2026. [CrossRef]

39. Gázquez, F.; Monteserín, A.; Obert, C.; Münker, C.; Fernández-Cortés, Á.; Calaforra, J.M. The absolute age and origin of the Giant Gypsum Geode of Pulpí (Almería, SE Spain). *Geosciences* **2022**, *12*, 144. [CrossRef]

40. Cotellucci, A.; Pellegrino, L.; Costa, E.; Bruno, M.; Dela Pierre, F.; Aquilano, D.; Destefanis, E.; Pastero, L. Effect of Different Evaporation Rates on Gypsum Habit: Mineralogical Implications for Natural Gypsum Deposits. *Cryst. Growth Des.* **2023**, *23*, 9094–9102. [CrossRef]

41. Cotellucci, A.; Otálora, F.; Canals, À.; Criado-Reyes, J.; Pellegrino, L.; Bruno, M.; Aquilano, D.; García-Ruiz, J.M.; Dela Pierre, F.; Pastero, L. $\bar{1}$01 contact twins in gypsum experimentally obtained from calcium carbonate enriched solutions: Mineralogical implications for natural gypsum deposits. *J. Appl. Crystal.* **2023**, *56*, 603–610. [CrossRef]

42. Natalicchio, M.; Pellegrino, L.; Clari, P.; Pastero, L.; Dela Pierre, F. Gypsum lithofacies and stratigraphic architecture of a Messinian marginal basin (Piedmont Basin, NW Italy). *Sediment. Geol.* **2021**, *425*, 106009. [CrossRef]

43. Costanzo, A.; Cipriani, M.; Feely, M.; Cianflone, G.; Dominici, R. Messinian twinned selenite from the Catanzaro Trough, Calabria Southern Italy: Filed, petrographic and fluid inclusion perspectives. *Carbonate Evaporite* **2019**, *34*, 743–756. [CrossRef]

44. Franchini-Angela, M.; Rinaudo, C. Influence of sodium and magnesium on the growth morphology of gypsum, CaSO$_4$·2H$_2$O. *Neues Jahrb. Mineral.-Abh.* **1989**, *160*, 105–115.

45. Rinaudo, C.; Zarka, A. X-ray Topographic study of synthetic single and twinned gypsum crystals. *J. Cryst. Growth* **1992**, *116*, 87–92. [CrossRef]

46. van Driessche, A.E.S.; Garcia-Ruiz, J.M.; Delgado-Lopez, J.M.; Sazaki, G. In situ observation of step dynamics on gypsum crystals. *Cryst. Growth Des.* **2010**, *10*, 3909–3915. [CrossRef]

47. Fürhedi-Milhofer, H. Spontaneous precipitation from electrolytic solutions. *Pure Appl. Chem.* **1981**, *53*, 2041–2055. [CrossRef]

48. He, S.; Oddo, J.E. The Nucleation Kinetics of Calcium Sulphate Dihydrate in NaCl Solutions up to 6m and 90 °C. *J. Colloid Interface Sci.* **1994**, *162*, 297–303. [CrossRef]

49. Söhnel, O.; Mullin, J.W. Interpretation of crystallization induction periods. *J. Colloid Interface Sci.* **1988**, *123*, 43–50. [CrossRef]

50. Kinsman, D.J.J. Gypsum and anhydrite of Recent age, Trucial Coast, Persian Gulf. In *Second Symposium on Salt*; Rau, J.L., Ed.; Northern Ohio Geological Society: Cleveland, OH, USA, 1966.

51. Koch, A.L. The logarithm in biology. *J. Theor. Biol.* **1969**, *12*, 276–290. [CrossRef]

52. Middleton, G.V. Generation of the Log-Normal Frequency Distribution in Sediments. In *Topics in Mathematical Geology*; Springer: Berlin/Heidelberg, Germany, 1970.

53. Crow, E.L.; Shimizu, K. *Lognormal Distributions: Theory and Applications*, 1st ed.; Marcel Dekker: New York, NY, USA, 1987.

54. Eberl, D.D.; Drits, V.A.; Srodón, J. Deducing growth mechanisms for minerals from the shapes of crystal size distributions. *Am. J. Sci.* **1998**, *298*, 499–533. [CrossRef]
55. Stawski, T.M.; Freeman, H.M.; van Driessche, A.E.S.; Hövelmann, J.; Besselink, R.; Wirth, R.; Benning, L.G. Particle-Mediated Nucleation Pathways Are Imprinted in the Internal Structure of Calcium Sulphate Single Crystals. *Cryst. Growth Des.* **2019**, *19*, 3714–3721. [CrossRef]
56. Mbogoro, M.M.; Peruffo, M.; Adobes-Vidal, M.; Field, E.L.; O'Connell, M.A.; Unwin, P.R. Quantitative 3D Visualization of the Growth of Individual Gypsum Microcrystals: Effect of Ca^{2+}/SO_4^{2-} Ratio on Kinetics and Crystal Morphology. *J. Phys. Chem. C* **2017**, *121*, 12726–12734. [CrossRef]